Supporting Information

Fabrication of two 2D Cu-based coordination polymers via secondary ligand adjustment and derived Cu/Cu_2O heterojunction for enhanced dye removal capacity

Wen-Ze Li,[a] Jing Li,[a] Hong-Tian Zhao,[a] Xiao-Sa Zhang,[a] Yu Liu,[a] Zhi-Tong Liu,[a] Hong-Xin Fu[a] and Jian Luan[b*]

[a] *College of Science, Shenyang University of Chemical Technology, Shenyang, 110142, P. R. China*

[b] *College of Sciences, Northeastern University, Shenyang, 110819, P. R. China*

E-mail: 2010044@stu.neu.edu.cn (J. Luan)

Table S1 Crystallographic data for Cu-CPs.

Complex	**Cu-CP-1**	**Cu-CP-2**
Formula	$C_{16}H_{14}CuN_4O_6$	$C_{20}H_{14}CuN_4O_6$
Formula wt	421.85	469.89
Crystal system	Monoclinic	Monoclinic
Space group	*P*21/*c*	*P*21/*c*
T (K)	296(2)	296(2)
a (Å)	5.5038(3)	9.7910(15)
b (Å)	15.3084(9)	6.3116(10)
c (Å)	9.9468(6)	28.379(4)
α (°)	90	90
β (°)	92.580(2)	93.082(4)
γ (°)	90	90
V (Å^3)	837.21(8)	1751.2(5)
Z	2	4
D_{calc} (g cm^{-3})	1.673	1.782
F(000)	430	956
θ_{max} (°)	25.06	28.35
R_{int}	0.0366	0.1119
R_1 [a] [$I > 2\sigma(I)$]	0.0398	0.0608
wR_2 [b] (all data)	0.0806	0.1214
GOF	1.011	1.000

[a] $R_1 = \Sigma||F_o|-|F_c||/\Sigma|F_o|$, [b] $wR_2 = \Sigma[w(F_o^2-F_c^2)^2]/\Sigma[w(F_o^2)^2]^{1/2}$.

Table S2 Selected bond distances (Å) and angles (°) for **Cu-CP-1**.

Cu(1)–O(1)#1	1.966(2)	Cu(1)–O(1)	1.966(2)
Cu(1)–N(1)#1	2.114(3)	Cu(1)–N(1)	2.114(3)
Cu(1)–O(2)#2	2.291(2)	Cu(1)–O(2)#3	2.291(2)
O(1)#1–Cu(1)–O(1)	180	O(1)#1–Cu(1)–N(1)#1	90.82(10)
O(1)–Cu(1)–N(1)#1	89.18(10)	O(1)#1–Cu(1)–N(1)	89.18(10)
O(1)–Cu(1)–N(1)	90.82(10)	N(1)#1–Cu(1)–N(1)	180
O(1)#1–Cu(1)–O(2)#2	78.69(8)	O(1)–Cu(1)–O(2)#2	101.31(8)
N(1)#1–Cu(1)–O(2)#2	90.56(9)	N(1)–Cu(1)–O(2)#2	89.44(9)
O(1)#1–Cu(1)–O(2)#3	101.31(8)	O(1)–Cu(1)–O(2)#3	78.69(8)
N(1)#1–Cu(1)–O(2)#3	89.44(9)	N(1)–Cu(1)–O(2)#3	90.55(9)
O(2)#2–Cu(1)–O(2)#3	179.998(1)		

Symmetry codes: #1 $-x + 1, -y, -z + 1$; #2 $x - 1, y, z$; #3 $-x + 2, -y, -z + 1$.

Table S3 Selected bond distances (Å) and angles (°) for **Cu-CP-2**.

Cu(1)–O(3)	1.929(3)	Cu(1)–O(1)	1.959(3)
Cu(1)–N(1)	2.000(3)	Cu(1)–N(2)#1	2.005(4)
Cu(1)–O(2)#2	2.353(3)	O(3)–Cu(1)–O(1)	84.54(13)
O(3)–Cu(1)–N(1)	88.61(13)	O(1)–Cu(1)–N(1)	171.05(14)
O(3)–Cu(1)–N(2)#1	166.52(14)	O(1)–Cu(1)–N(2)#1	93.40(14)
N(1)–Cu(1)–N(2)#1	91.92(14)	O(3)–Cu(1)–O(2)#2	94.41(12)
O(1)–Cu(1)–O(2)#2	94.47(12)	N(1)–Cu(1)–O(2)#2	91.78(13)
N(2)#1–Cu(1)–O(2)#2	99.04(13)		

Symmetry codes: #1 $-x + 1, -y - 1, -z + 1$; #2 $-x, y - 1/2, -z + 1/2$.

Table S4 Table of distributions of element contents by SEM-EDX for the materials.

Material	Cu (wt%)	C (wt%)	O (wt%)	N (wt%)	S (wt%)
Cu-CP-1-800	93.82	4.28	1.90	—	—
Cu-CP-2-800	71.99	17.74	10.27	—	—
Cu@C-1	69.95	26.75	3.30	—	—
Cu@C-2	44.28	53.03	2.69	—	—
Cu@N-1	56.58	38.09	5.33	—	—
Cu@N-2	42.41	47.71	9.88	—	—
Cu@S-1	68.22	28.32	3.46	—	—
Cu@S-2	46.91	49.65	3.44	—	—

Table S5 Organic dyes with different charge types and sizes.

Dye	Formula	Charge type	Size (nm × nm × nm)
Methylene Blue (MB)	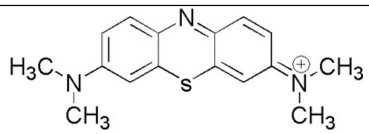	Cationic	0.40 × 0.79 × 1.63
Rhodamine B (RhB)	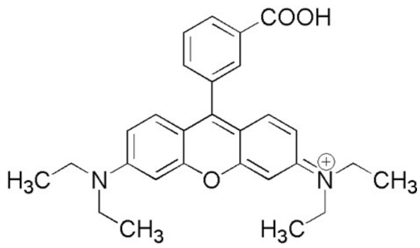	Cationic	0.68 × 1.18 × 1.57
Methyl Orange (MO)	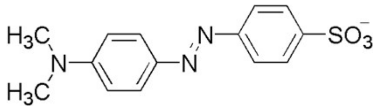	Anionic	0.53 × 0.73 × 1.74
Congo Red (CR)	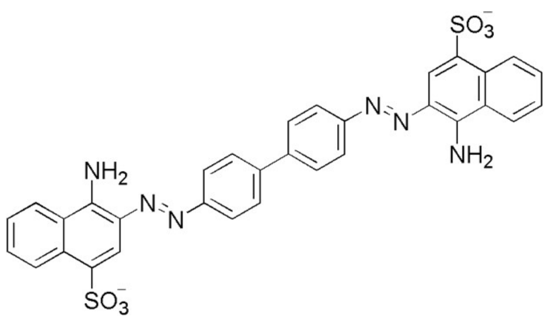	Anionic	0.39 × 0.86 × 2.61

Table S6 List of zeta potential values of the samples.

Material	**Cu-CP-1**	**Cu@C-1**	**Cu@N-1**	**Cu@S-1**	**Cu-CP-2**	**Cu@C-2**	**Cu@S-2**	**Cu@S-2**
Zeta potential value (mV)	2.97	–0.10	–0.46	0.70	1.23	–0.23	–1.60	0.21

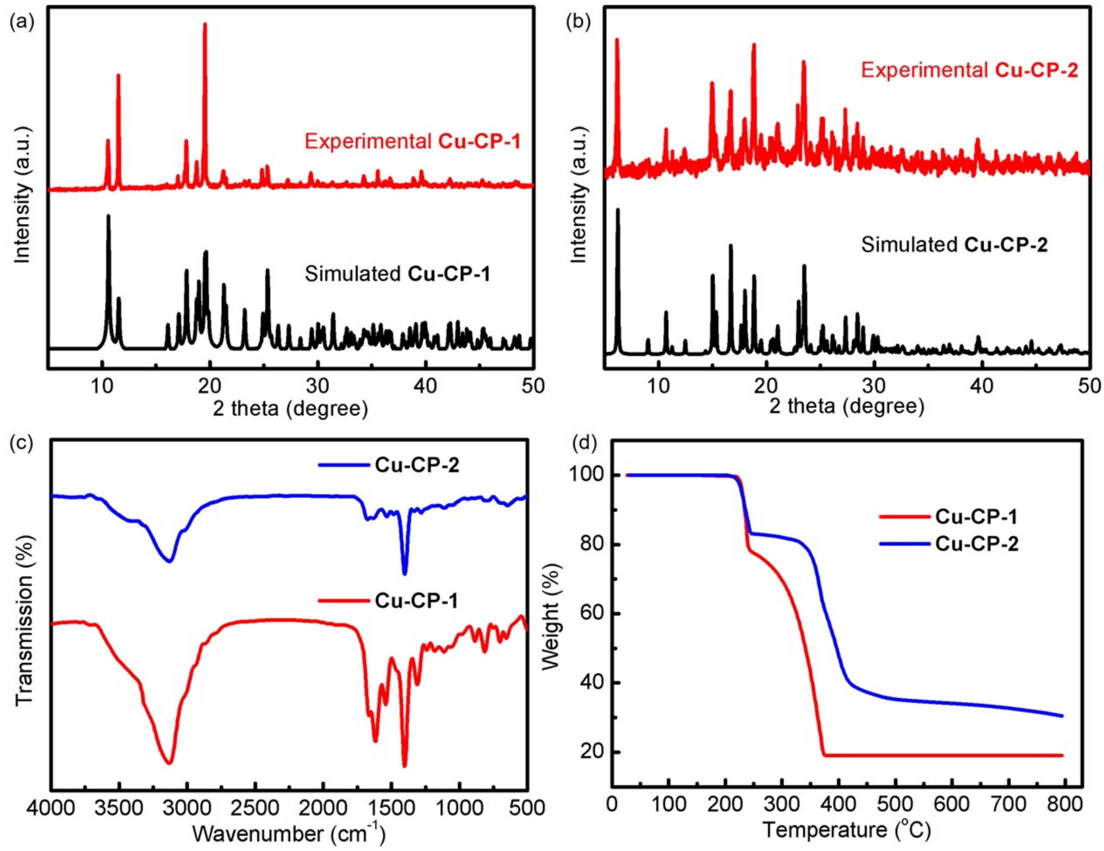

Fig. S1 (a) The PXRD patterns of simulated and fresh sample for **Cu-CP-1**; (b) The PXRD patterns of simulated and fresh sample for **Cu-CP-2**; (c) The IR spectra of **Cu-CP-1** and **Cu-CP-2**; (d) The TG curve of **Cu-CP-1** and **Cu-CP-2**.

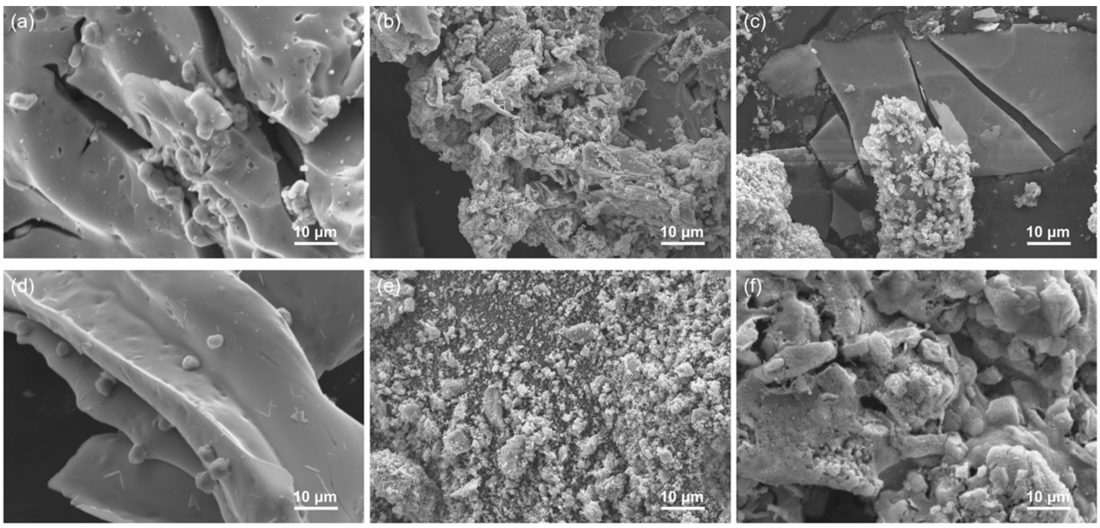

Fig. S2 Typical SEM images of **Cu@C-1** (a), **Cu@N-1** (b), **Cu@S-1** (c), **Cu@C-2** (d), **Cu@N-2** (e), and **Cu@S-2** (f).

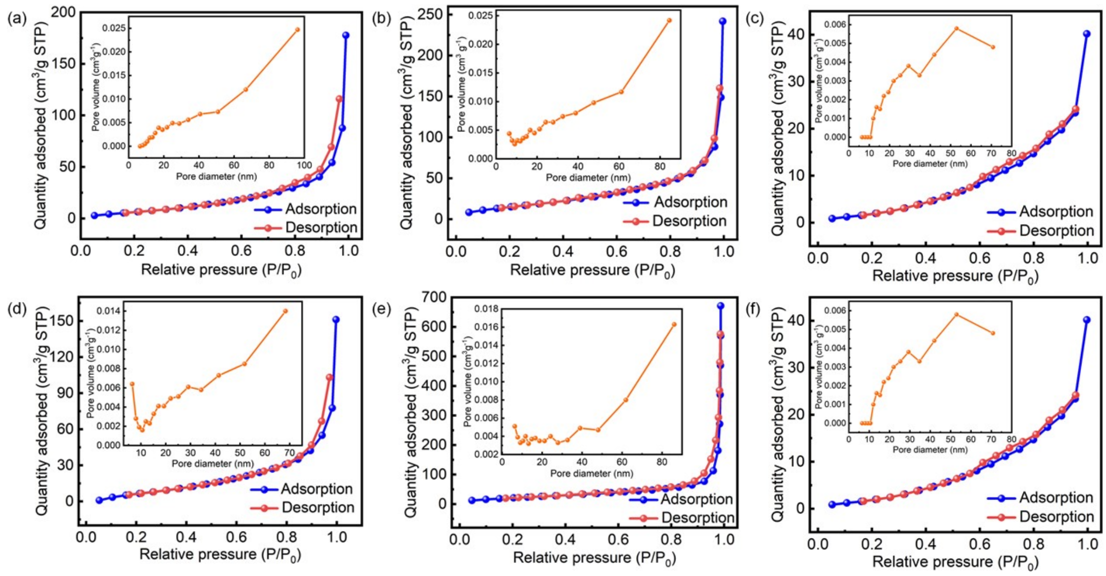

Fig. S3 Nitrogen adsorption and desorption isotherms (inset: the pore size distribution) of **Cu@C-1** (a), **Cu@N-1** (b), **Cu@S-1** (c), **Cu@C-2** (d), **Cu@N-2** (e), and **Cu@S-2** (f).

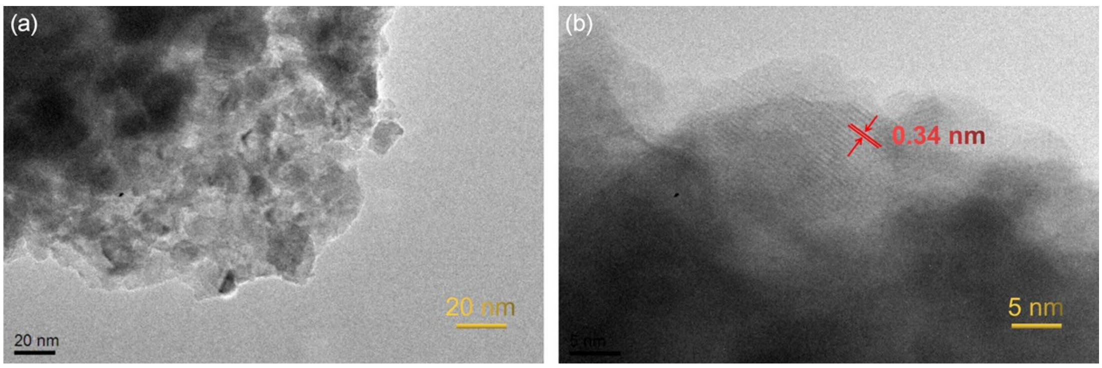

Fig. S4 Typical HRTEM images of **Cu@N-2**: (a) Lower magnification; (b) Higher magnification..

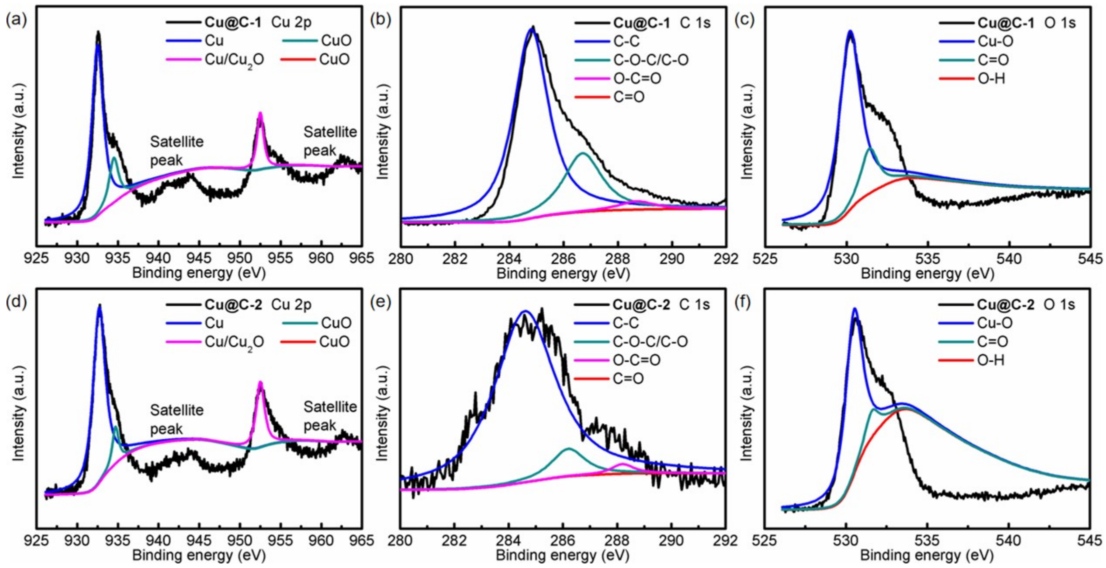

Fig. S5 XPS analysis of the Cu 2p (a), C 1s (b) and O 1s (c) spectra of **Cu@C-1**. XPS analysis of the Cu 2p (d), C 1s (e) and O 1s (f) spectra of **Cu@C-2**.

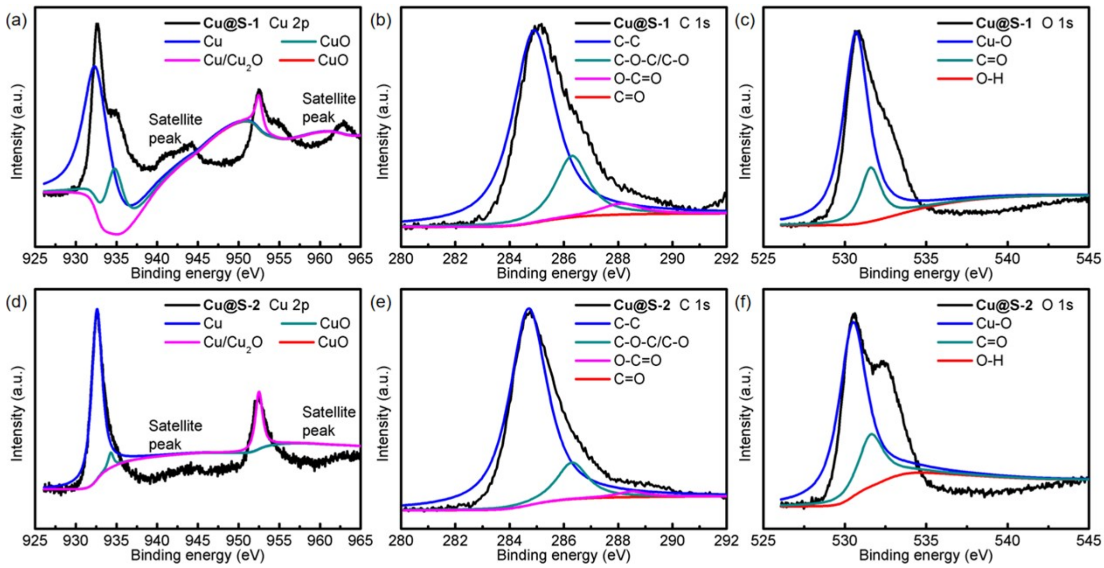

Fig. S6 XPS analysis of the Cu 2p (a), C 1s (b) and O 1s (c) spectra of **Cu@S-1**. XPS analysis of the Cu 2p (d), C 1s (e) and O 1s (f) spectra of **Cu@S-2**.

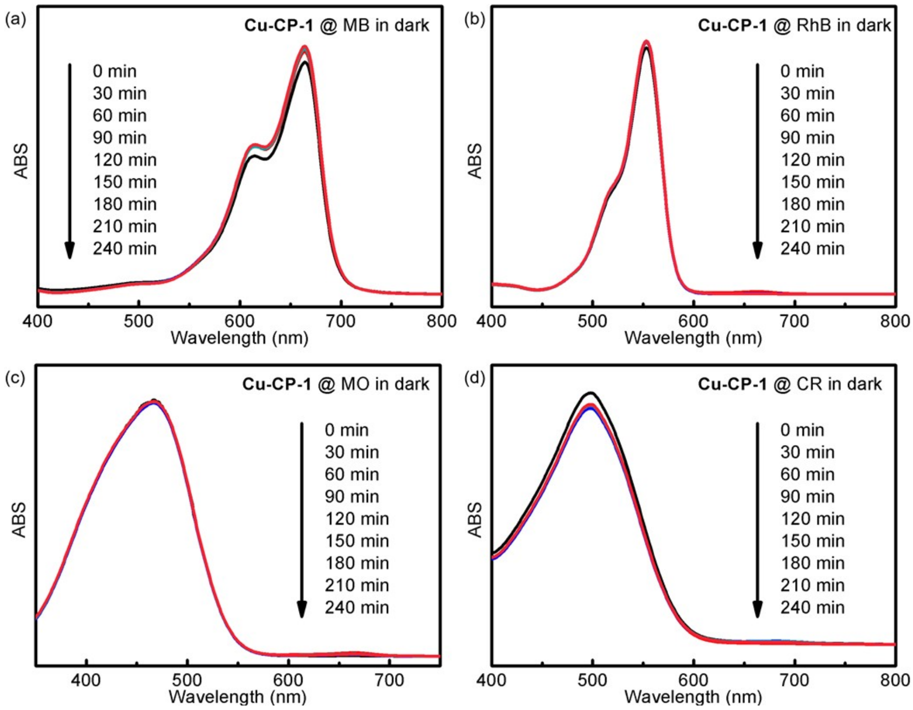

Fig. S7 UV-vis spectra of MB (a), RhB (b), MO (c) and CR (d) solutions recorded after different adsorption times with **Cu-CP-1**.

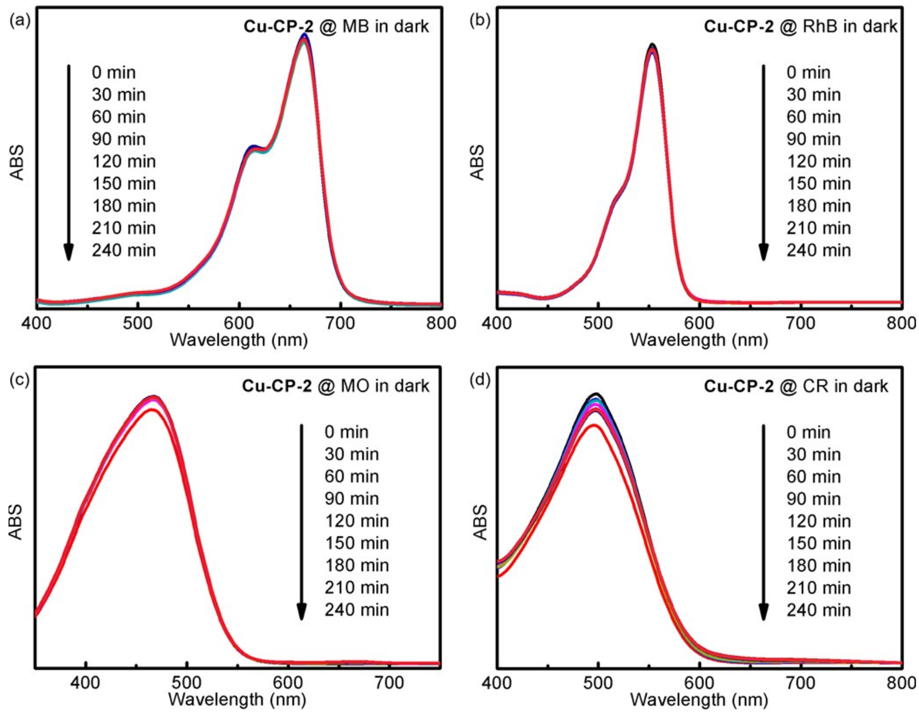

Fig. S8 UV-vis spectra of MB (a), RhB (b), MO (c) and CR (d) solutions recorded after different adsorption times with **Cu-CP-2**.

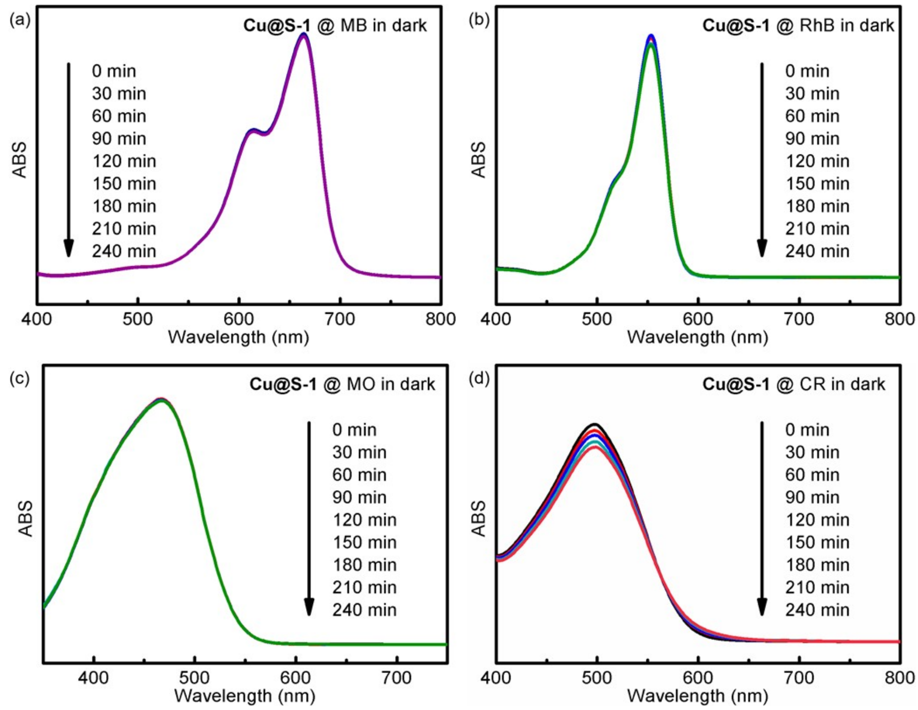

Fig. S9 UV-vis spectra of MB (a), RhB (b), MO (c) and CR (d) solutions recorded after different adsorption times with **Cu@S-1**.

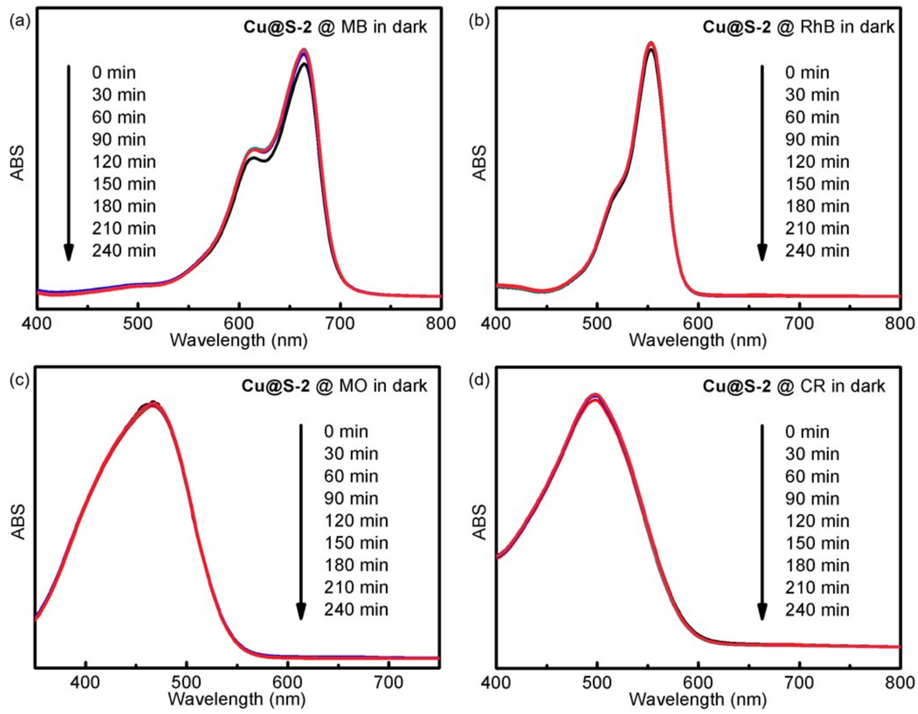

Fig. S10 UV-vis spectra of MB (a), RhB (b), MO (c) and CR (d) solutions recorded after different adsorption times with **Cu@S-2**.

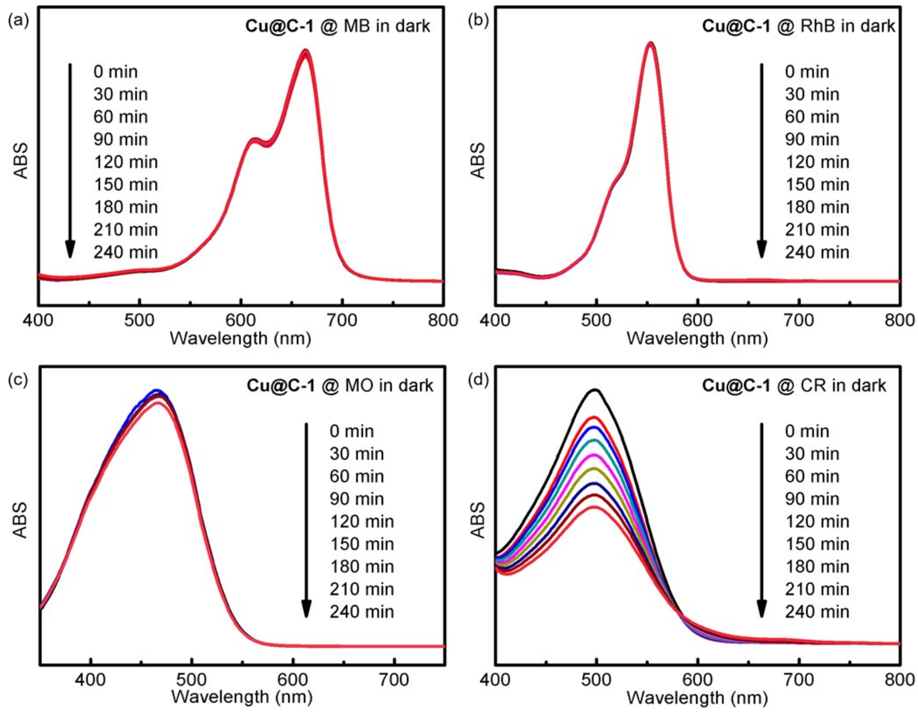

Fig. S11 UV-vis spectra of MB (a), RhB (b), MO (c) and CR (d) solutions recorded after different adsorption times with **Cu@C-1**.

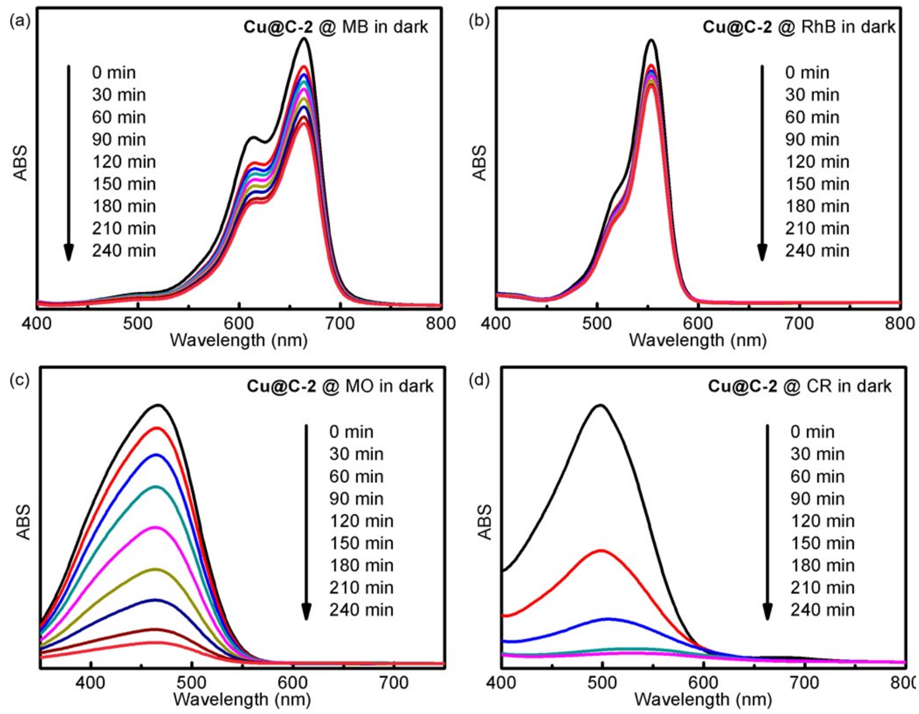

Fig. S12 UV-vis spectra of MB (a), RhB (b), MO (c) and CR (d) solutions recorded after different adsorption times with **Cu@C-2**.

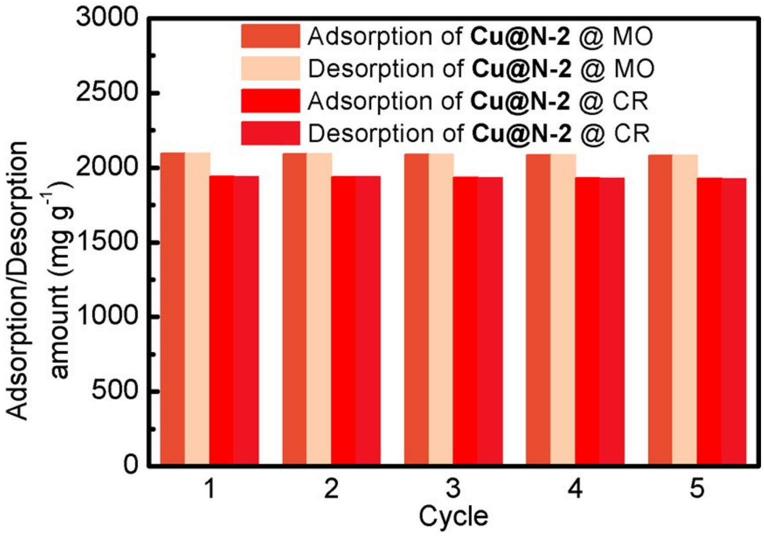

Fig. S13 The cycling stability of the adsorption/desorption of dyes on the **Cu@N-2**.

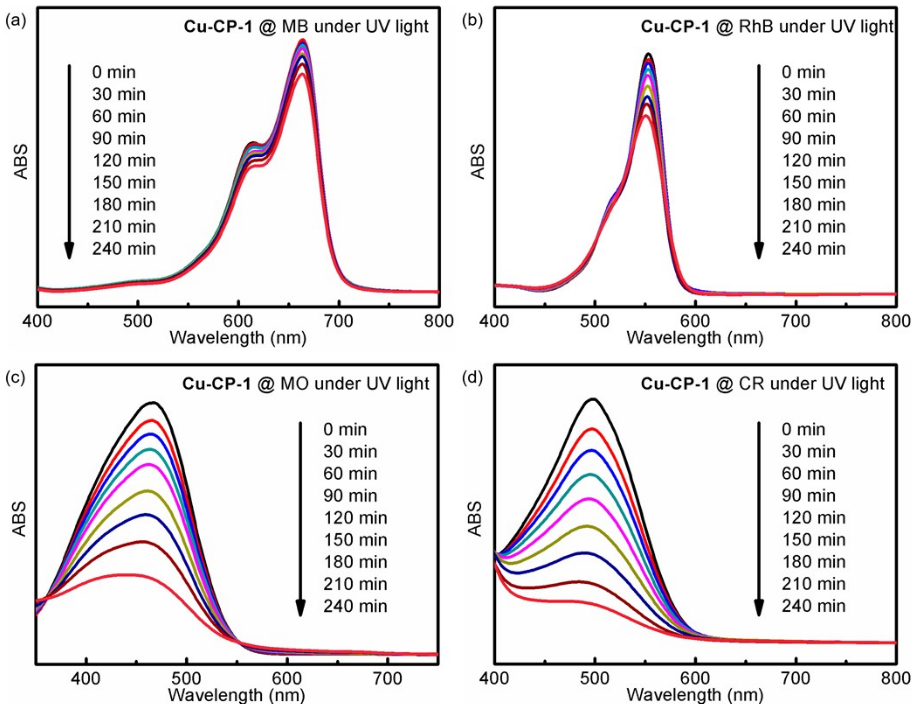

Fig. S14 UV-vis spectra of MB (a), RhB (b), MO (c) and CR (d) solutions recorded after different photocatalytic degradation times with **Cu-CP-1**.

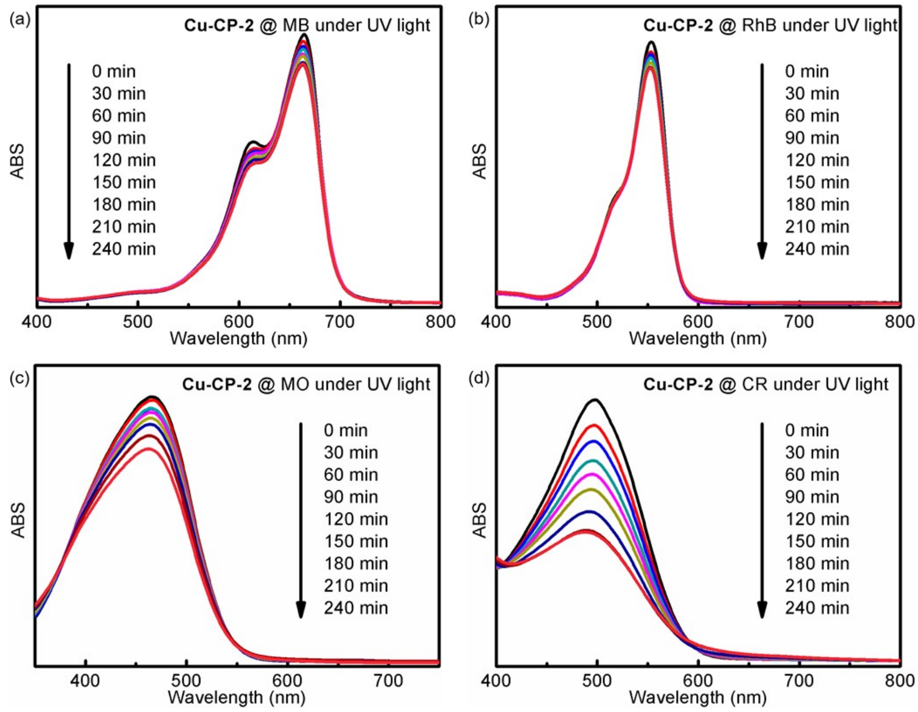

Fig. S15 UV-vis spectra of MB (a), RhB (b), MO (c) and CR (d) solutions recorded after different photocatalytic degradation times with **Cu-CP-2**.

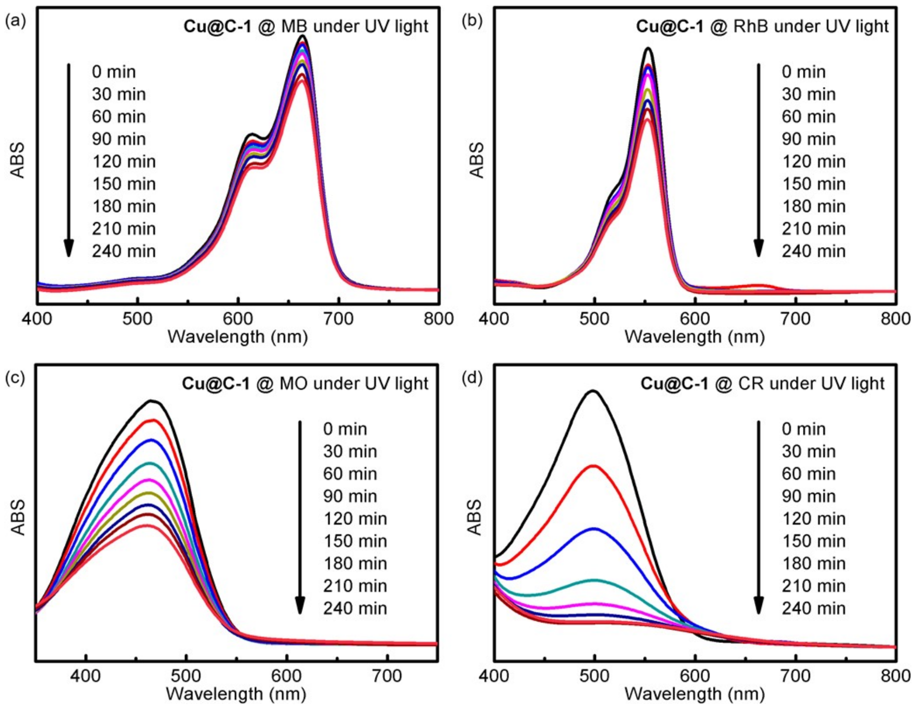

Fig. S16 UV-vis spectra of MB (a), RhB (b), MO (c) and CR (d) solutions recorded after different photocatalytic degradation times with **Cu@C-1**.

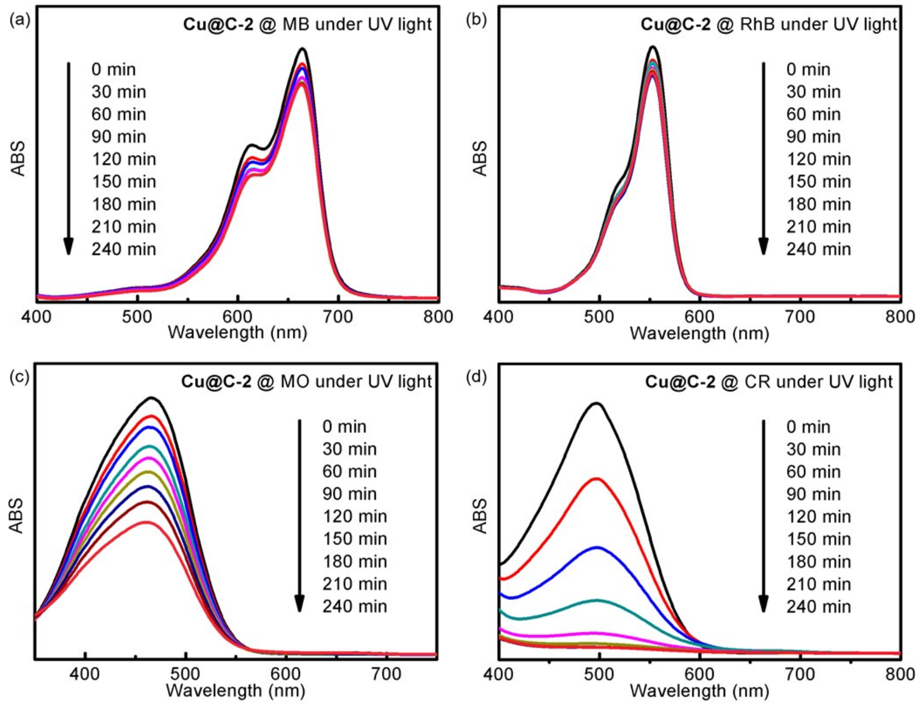

Fig. S17 UV-vis spectra of MB (a), RhB (b), MO (c) and CR (d) solutions recorded after different photocatalytic degradation times with **Cu@C-2**.

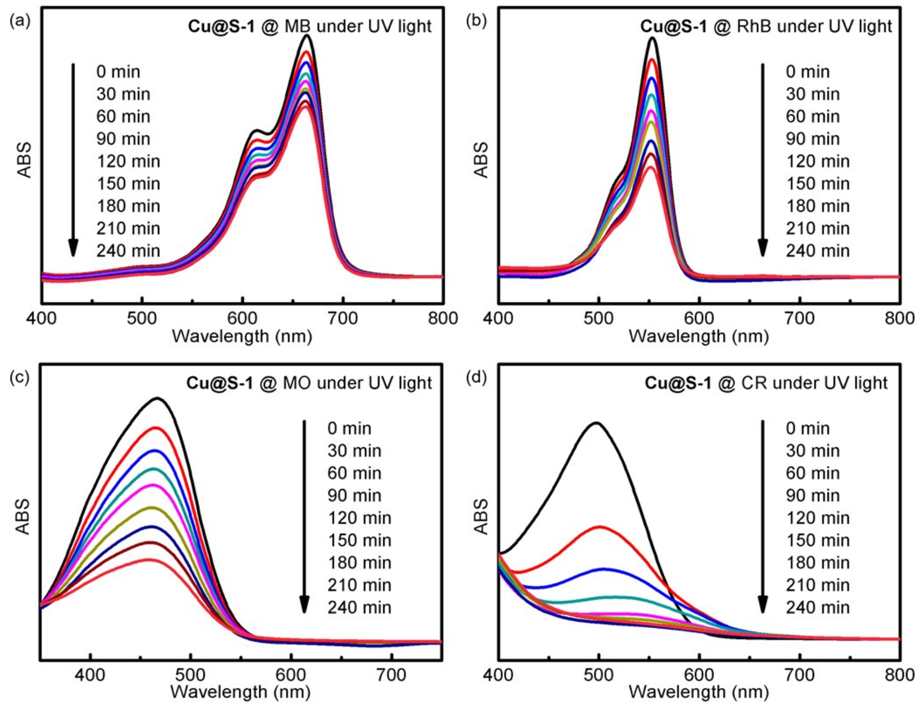

Fig. S18 UV-vis spectra of MB (a), RhB (b), MO (c) and CR (d) solutions recorded after different photocatalytic degradation times with **Cu@S-1**.

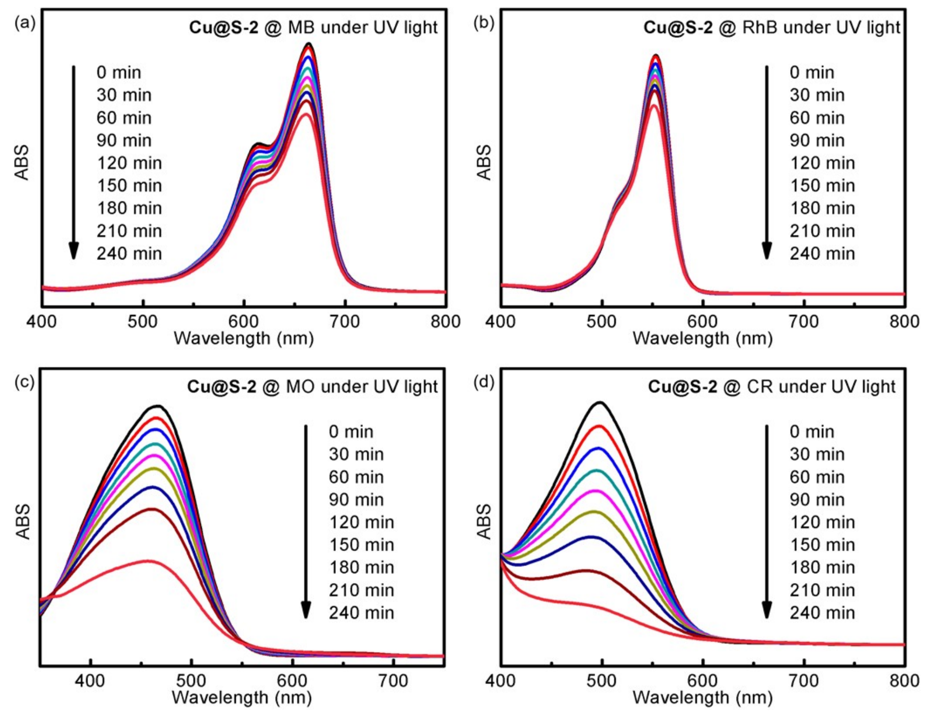

Fig. S19 UV-vis spectra of MB (a), RhB (b), MO (c) and CR (d) solutions recorded after different photocatalytic degradation times with **Cu@S-2**.

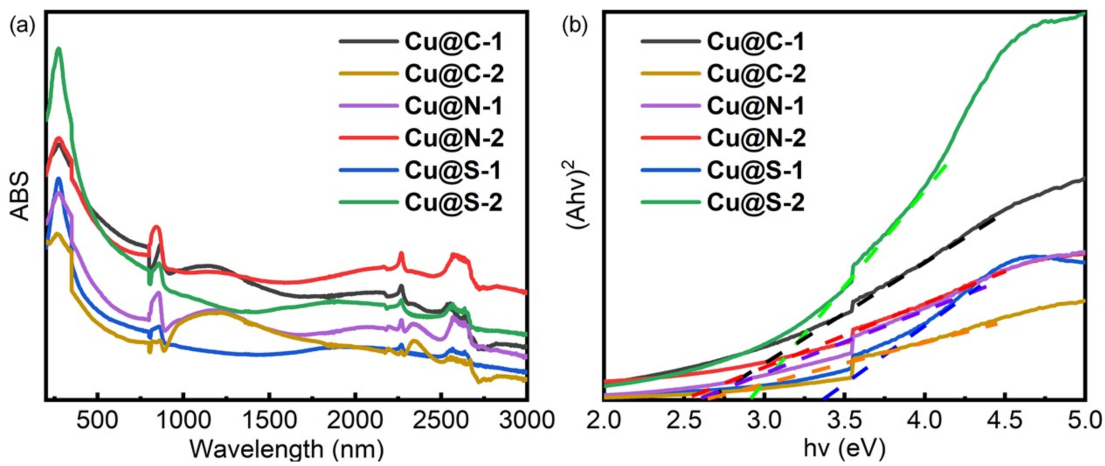

Fig. S20 UV–vis absorption spectra (a) and bandgap energies (b) of Cu/Cu_2O heterojunctions.

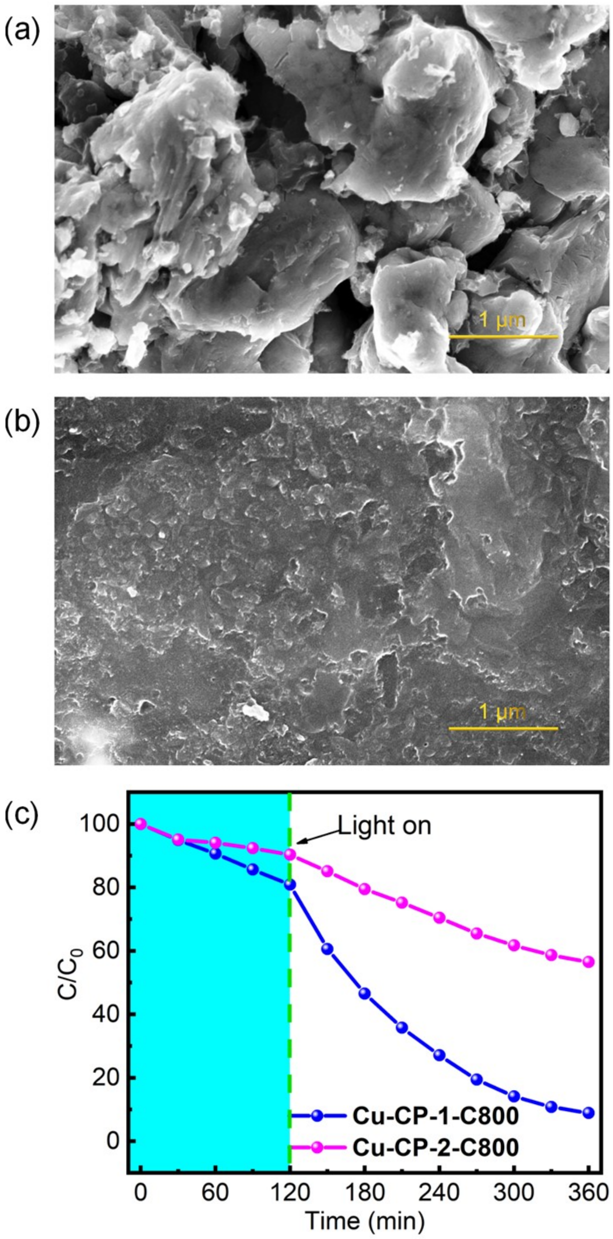

Fig. S21 Typical SEM images of **Cu-CP-1-C800** (a) and **Cu-CP-2-C800** (b). (c) The photocatalytic degradation rates of CR at different time points during exposure to **Cu-CP-1-C800** and **Cu-CP-2-C800**.

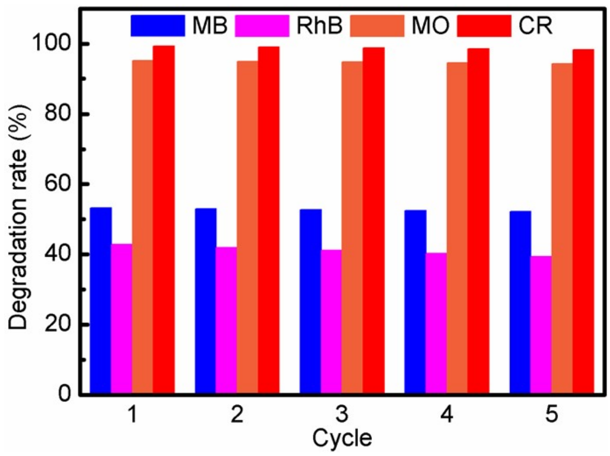

Fig. S22 The reproducibility of the photocatalyst **Cu@N-2** for dyes.

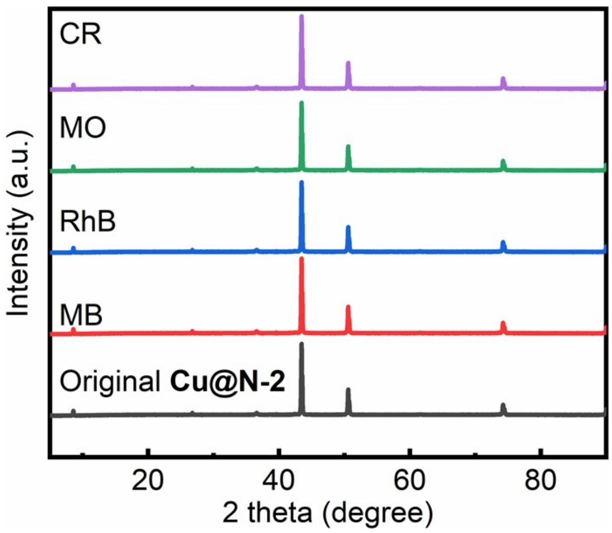

Fig. S23 The PXRD patterns before and after recycle for five times of the photocatalyst **Cu@N-2** for dyes.